



This is a repository copy of *The effect of magnesia and lime on the durability of synthetic basaltic glasses*.

White Rose Research Online URL for this paper:
<https://eprints.whiterose.ac.uk/id/eprint/225082/>

Version: Accepted Version

Article:

Mansfield, J.T., Tang, C.T., Thorpe, C.L. et al. (3 more authors) (2025) The effect of magnesia and lime on the durability of synthetic basaltic glasses. *Journal of Non-Crystalline Solids*, 656. 123500. ISSN 0022-3093

<https://doi.org/10.1016/j.jnoncrysol.2025.123500>

© 2025 The Authors. Except as otherwise noted, this author-accepted version of a journal article published in *Journal of Non-Crystalline Solids* is made available via the University of Sheffield Research Publications and Copyright Policy under the terms of the Creative Commons Attribution 4.0 International License (CC-BY 4.0), which permits unrestricted use, distribution and reproduction in any medium, provided the original work is properly cited. To view a copy of this licence, visit <http://creativecommons.org/licenses/by/4.0/>

Reuse

This article is distributed under the terms of the Creative Commons Attribution (CC BY) licence. This licence allows you to distribute, remix, tweak, and build upon the work, even commercially, as long as you credit the authors for the original work. More information and the full terms of the licence here:
<https://creativecommons.org/licenses/>

Takedown

If you consider content in White Rose Research Online to be in breach of UK law, please notify us by emailing eprints@whiterose.ac.uk including the URL of the record and the reason for the withdrawal request.



eprints@whiterose.ac.uk
<https://eprints.whiterose.ac.uk/>

The effect of magnesia and lime on the durability of synthetic basaltic glasses

James T Mansfield^{1,*}, CT Tang¹, Clare L. Thorpe¹, Claire L. Corkhill^{1,2}, Mike T. Harrison³ and Russell J Hand¹

¹SL, School of Chemical, Materials and Biological Engineering, University of Sheffield, Sir Robert Hadfield Building, Mappin Street, Sheffield, S1 3JD, UK

²School of Earth Sciences, University of Bristol, Wills Memorial Building, Queens Road, Bristol BS8 1RJ, UK

³United Kingdom National Nuclear Laboratory, Sellafield, Seascale, Cumbria, UK

Abstract

The effect of varying $\frac{[\text{MgO}]}{[\text{MgO}] + [\text{CaO}]}$ ratios on the chemical durability of a series of synthetic basaltic glasses is examined via monolith (MCC-1) and powder (PCT-B) tests for times up to 1800 days (MCC-1) or 224 days (PCT-B). It is demonstrated that the magnesium-rich compositions generally have a lower durability than the calcium rich ones. For the shorter MCC-1 tests the normalised losses of all elements increase with time but at longer times both Mg and Al are removed from solution. Higher Mg content basaltic glasses developed thicker alteration layers with reduced Al and Mg contents along with secondary precipitates (potentially aluminous hectorite clays). The laboratory assessed alteration rates, based on alteration layer thicknesses from the accelerated MCC-1 tests at 90 °C, are demonstrated to be at least 2 orders of magnitude greater than the alteration rates reported for natural basalts in a range of continental and oceanic settings.

1 Introduction and background

To gain insight into the long term performance of vitrified nuclear waste in a disposal environment, natural ‘analogue’ glasses have been studied by a number of authors (see, for example, [1-3]). Natural glasses are typically aluminosilicates (see, for example, [4]) that, unlike many nuclear waste glasses, do not contain boron oxide, however they do enable comparison of glass behaviour in relatively short term laboratory experiments with their behaviour over extended timescales in the natural environment. In particular basaltic glasses have been the subject of a number of analogue studies as, despite the lack of boron oxide, they are considered to be compositionally similar to nuclear waste glasses (see, for example, [5, 6]).

From 1964 until 2015 the UK operated a series of Magnox fission reactors. These reactors used a non-enriched metallic uranium fuel with a magnesium alloy cladding. During this period the UK also operated a closed nuclear fuel cycle with reprocessing of the spent Magnox fuel and, latterly, spent oxide fuel from the advanced gas cooled reactors (AGRs) and light water reactors [7]. The highly active liquor (HAL) resulting from the fuel reprocessing has been vitrified using the “Mixture Windscale” (MW) base glass, although more recently a modified base glass composition referred to as CaZn glass has also been used [8]. The HAL being incorporated into the vitrified product ranges from a 25:75 Magnox:oxide HAL mix to 100% Magnox HAL [7]. As a consequence, UK vitrified high level waste products are relatively magnesia rich when compared both to nuclear waste glasses produced in other

* Now at EDF Energy, Hinkley Point Visitor Centre, Cannington Court, Church Street, Bridgwater, Somerset, TA5 2HA

countries [9], an exception being French AVM glasses [10-12], and also to natural analogue glasses, such as basaltic glasses.

Glass dissolution in stagnant/semi-stagnant conditions is widely considered to consist of three major stages [13]. In the classical, stage based model, during stage I ion exchange of glass modifier ions (primarily alkali ions) with H_3O^+ ions and network hydrolysis are the primary processes that occur [14, 15]. With the development of alteration layers on the glass surface, as well as saturation of the solution adjacent to the glass, the rate of alteration drops resulting in stage II where the so-called residual or final rate of alteration is observed [15]. The detailed mechanisms that explain the development of the alteration layers, especially the porous surface gel layer, have been the subject of significant debate in the literature (see, for example, [16-19]) and there are indications that minor components can have significant effects on the composition and passivating nature of the surface layers observed [20]. At longer times there may be a transition from stage II to stage III where precipitation of less soluble phases onto the alteration layers leads to a resumption of more rapid alteration (see, for example, [21]), where alteration rates have been reported to be higher than stage II but less than the initial rate [22]. In magnesium containing systems reduction in initial dissolution rates associated with the role of Mg in the glass structure increasing its intrinsic durability has been reported [23]. The precipitation of magnesium phyllosilicates that remove Si from solution has been associated with higher residual rates [11, 12, 24, 25] and it has been suggested that their precipitation may be associated with the transition to stage III behaviour [26]. Hence, there is a need to develop a deeper understanding of the impact of Mg on glass durability, including on analogue compositions.

The reported studies on basaltic glasses have molar $\frac{[MgO]}{[MgO]+[CaO]}$ ratios of 0.38 – 0.52 [3, 5, 27], whereas 25 wt% waste loading of a simulant Magnox waste 'calcine' (WRW17) in MW gives an $\frac{[MgO]}{[MgO]+[CaO]}$ ratio of 0.97 [28]. Hence the current work examines the durability behaviour of a series of laboratory made basaltic glass compositions with $\frac{[MgO]}{[MgO]+[CaO]}$ ratios varying from 0 to 1, but with otherwise nominally fixed compositions, to establish the impact of increasing the MgO content on the performance of such glasses under accelerated laboratory test conditions.

2 Experimental

A series of 5 basaltic glasses based on the composition given by Techer *et al.* [6], with fixed total alkaline earth contents, but with varying quantities of magnesia and lime were prepared. Sample naming is of the form $xMg:(100-x)Ca$ reflecting the measured ratio of MgO:CaO. Glass batches, each designed to produce 300 g glass, were prepared from high quality glass making sand (Loch Aline; 99.5%); sodium carbonate (Sigma Aldrich; 99.9%); calcium carbonate (Sigma Aldrich; 99.9%); potassium carbonate (Alfa Aesar, 99%); hydrated magnesium carbonate (Fisher, 99%); aluminium trihydroxide (Sigma Aldrich, 99%); ammonium dihydrogen phosphate (Alfa Aesar, 98%); titanium dioxide (Sigma Aldrich, 99.8%); strontium nitrate (Aldrich, $\geq 98\%$); lithium carbonate (Alfa Aesar, 99%); iron (III) oxide (Alfa Aesar, 98%) and manganese (II) carbonate (Alfa Aesar, 99.8%).

The glasses were produced from powdered raw materials by heating at 1450 °C in a Pt crucible. Each composition was melted for a total of 5 hours in an electric furnace; 1 hour to batch free followed by 4 hours stirring. The melts were cast into pre-heated mild steel moulds and then annealed at 670 °C for 1 hour. After annealing the glass ingots were furnace cooled to room temperature.

2.1 Glass characterisation

2.1.1 Composition

Following an HF digest, inductively coupled plasma-optical emission spectroscopy (ICP-OES) was used to determine the compositions of the as-made glasses. The batched and measured glass compositions are given in Table 1.

Table 1: Measured (ICP-OES) and batched (bracketed values) compositions of the laboratory made basaltic glasses studied here. All data converted to mol. % and normalised to 100 mol. %. *K₂O was below the ICP-OES detection limit – the 0.12 mol. % value is therefore an upper bound. Errors in analysis estimated as ± 3 %. Measured density values are also reported.

Oxide	Oxide mol. % measured (batched)				
	2Ca98Mg	33Ca67Mg	46Ca54Mg	72Ca28Mg	100Ca0Mg
Na ₂ O	3.07 (2.80)	3.01 (2.80)	3.26 (2.80)	2.94 (2.80)	3.05 (2.80)
Li ₂ O	1.81 (2.17)	1.75 (2.17)	1.81 (2.17)	1.74 (2.17)	1.78 (2.17)
K ₂ O	<0.12* (0.13)	<0.12* (0.13)	<0.12* (0.13)	<0.12* (0.13)	<0.12* (0.13)
MgO	23.41 (25.93)	16.32 (18.15)	14.11 (15.09)	6.67 (7.78)	0.00 (0.00)
CaO	0.36 (0.00)	8.12 (7.78)	11.78 (10.84)	17.02 (18.15)	24.77 (25.93)
SrO	0.35 (0.23)	0.34 (0.23)	0.36 (0.23)	0.33 (0.23)	0.34 (0.23)
MnO	0.16 (0.14)	0.15 (0.14)	0.16 (0.14)	0.15 (0.14)	0.15 (0.14)
Al ₂ O ₃	9.12 (9.41)	9.19 (9.41)	7.61 (9.41)	8.26 (9.41)	7.89 (9.41)
Fe ₂ O ₃	4.56 (4.41)	4.43 (4.41)	4.55 (4.41)	4.36 (4.41)	4.51 (4.41)
TiO ₂	1.53 (1.44)	1.50 (1.44)	1.51 (1.44)	1.44 (1.44)	1.49 (1.44)
P ₂ O ₅	0.08 (0.05)	0.08 (0.05)	0.09 (0.05)	0.08 (0.05)	0.12 (0.05)
SiO ₂	55.44 (53.29)	55.00 (53.29)	54.63 (53.29)	56.89 (53.29)	55.79 (53.29)
$\frac{[\text{MgO}]}{[\text{MgO}] + [\text{CaO}]}$	0.985 (1.000)	0.668 (0.700)	0.545 (0.581)	0.281 (0.300)	0.000 (0.000)
Density / 10 ³ kg m ⁻³	2.758 \pm 0.001	2.785 \pm 0.001	2.806 \pm 0.001	2.826 \pm 0.001	2.852 \pm 0.002

2.1.2 Density

Glass densities were measured using gas pycnometry. Approximately one gram of glass powder (< 75 μm) was measured per composition using an AccuPyc II 1340 Gas Displacement Pycnometry System. The average density across ten purge cycles was calculated using helium introduced at 2.23 kPa s⁻¹.

2.1.3 Raman spectroscopy

Raman spectra between 100-2000 cm⁻¹ were collected using a Renishaw InVia Raman microscope with a grating of 2 400 lines mm⁻¹. Spectra were excited for 10 seconds using a 514 nm line of a 25 mW argon ion laser at 80% power, with 10 acquisitions per sampled area and an image magnification of 50 \times .

2.2 Durability testing

Durability testing was conducted using both the MCC-1 [29] and PCT-B [30] and protocols. MCC-1 testing was conducted on 2Ca98Mg, 46Ca54Mg and 100Ca0Mg glasses only, whereas PCT-B was conducted on all five glasses.

2.2.1 MCC-1 testing

For MCC-1 the glass ingots were cut into $\sim 10 \times 10 \times 5$ mm monoliths, progressively ground and polished using P600, P800 and P1200 grit SiC abrasive papers followed by 6, 3 and 1 μm oil based

diamond suspensions. The polished monoliths were sequentially cleaned using UHQ water and isopropanol before drying at 90 °C for ~ 12 h. Prepared monoliths were placed into Savillex 60 ml perfluoralkoxy (PFA) Teflon standard vessels which had been cleaned as per the ASTM standard [29] containing a support screen ('basket') of the same material. UHQ was added in appropriate quantities to these vessels to give a sample surface area to volume of solution (SA/V) of 10 m⁻¹; the required leachant volume for each timestep was calculated based on the average geometric surface area measured for all monoliths of a given timestep.

The sealed vessels were placed into a GenLab MINO/40 oven at 90 ± 2 °C for 28, 56, 112, 224, 461 (2Ca98Mg and 100Ca0Mg) or 468 (46Ca54Mg), and 672 d. A temperature of 90 °C was utilised to allow comparison with the earlier studies on basalts of Techer and co-workers [6, 31] and to maximise probable dissolution rates. In addition, a single 2Ca98Mg and a single 100Ca0Mg sample remained under test for an extended period of 1800 d. After testing, the vessels were removed from the oven, weighed and allowed to cool to room temperature before the monolith was removed and allowed to air-dry for 24-48 hours. The solution pH was measured on a 10-15 ml aliquot of the solution. A second, similarly sized, aliquot was forced (using a polyethylene/polypropylene syringe) through a Puradisc 0.2 µm cellulose acetate filter and then acidified with 1 vol. % ultrapure concentrated nitric acid to avoid precipitation of secondary phases prior to elemental analysis.

The dried monoliths were lifted from their support screens, using soft plastic tweezers; some localised damage to alteration layers during this process was unavoidable, but restricted to the area in contact with tweezers. Two of the triplicate monoliths per composition/timestep were placed into plastic sample clips before being mounted in an epoxy based mounting resin (80% Buehler EpoxiCure™ 2 Epoxy Resin thoroughly mixed with 20% Buehler EpoxiCure™ 2 Epoxy Hardener).

2.2.2 PCT-B testing

For PCT the glass samples were size-reduced using a percussion pestle and mortar and then sieved to obtain the 75-150 µm size fraction. The powder samples were sequentially cleaned in Milli-Q® ultra-high quality (UHQ) water and isopropanol to remove adhered fines using an ultrasonic bath until each waste solution was visibly particulate-free (~ 30-60 min per washing stage). After oven-drying (at 90 °C for ~ 8 hours), powder density was measured using pycnometry and used to calculate the sample volume (assuming spherical particles) required to achieve an SA/V of 2 000 m⁻¹. The weighed powders were added to 15 ml PFA test vessels. 10 ml of UHQ water was added and the vessels were closed, lids tightened and placed into a GenLab MINO/40 oven at 50 ± 2 °C for 7, 14, 28, 56, 112 or 224 d; the lower experimental temperature of 50 °C was selected for the PCT experiments after initial trials at 90 °C resulted in unacceptably high evaporative losses. On removal from the oven vessels were allowed to cool to room temperature and then weighed. A 7 ml aliquot of the solution was filtered and acidified with 1 vol. % ultrapure nitric acid, whilst the remaining 2-3 ml was removed and used for pH measurement. Vessels (containing glass powder and minimal leachate) were then placed into a drying oven at 30 °C for 8 – 48 hours before the powder was removed. SEM samples were prepared by mixing ~ 0.2 g of the dried powder in a ~ 50:50 ratio with the same epoxy system used for the MCC-1 samples, before the resulting mixture was transferred into a ~ 0.5 mm diameter cylindrical plastic sample clip. Additional epoxy/hardener was poured around this.

2.2.3 Leachate analysis

Leachate pH was measured conducted at room temperature (~ 20 °C) using a Mettler Toledo Five Easy Plus reader and Mettler Toledo LE422 probe calibrated using pH buffers at pH 4, 7 and 10.

ICP-OES was used to quantify the elemental contents of leachates post-dissolution. Leachate analysis was conducted using a ThermoFisher iCAPDuo 63000 ICP-OES equipped with a fused silica torch. The

measured leachate concentrations were blank corrected and also corrected for any evaporative losses during testing (obtained from the post-dissolution vessel mass). The normalised mass loss of element i (NL_i in g m^{-2}) is given by

$$NL_i = \frac{C_i - C_{i,b}}{f_i (SA/V)} \quad (1)$$

where C_i and $C_{i,b}$ are the average concentrations (in g m^{-3}) of element i in the analysed leachates of the triplicate sample vessels and duplicate blank vessels respectively and f_i (unitless) is the fraction of element i in the initial glass composition.

2.3 Scanning electron microscopy (SEM)

The epoxy-mounted MCC-1 and PCT samples were successively ground and polished to a $1 \mu\text{m}$ finish using P600, P800 and P1200 grit SiC abrasive papers with isopropanol as a lubricant followed by 6, 3 and $1 \mu\text{m}$ oil based diamond suspensions. Copper-tape was applied to electrically connect the bottom and top of the resin-mounted samples which were then carbon-coated using a Quorum Q150T ES Plus.

The samples were characterised with a Hitachi TM3030 Plus scanning electron microscope (SEM) coupled with Bruker Quantax 70 energy dispersive spectrometer (EDS). An accelerating voltage of 15 kV and a beam current of 2×10^{-9} A was used with a working distance of 7-9 mm. EDS spectra were collected for at least ten minutes, with back-scattered electron (BSE) images collected at the maximum available resolution.

2.4 Alteration layer thicknesses

Alteration layer thickness was assessed in a semi-automated manner using Object Research Systems' Dragonfly software [32]. SEM photomicrographs were imported into Dragonfly as a single greyscale channel (*i.e.* with RGB channels assumed identical) with an 8-bit colour depth. Each pixel was thus automatically assigned a greyscale value from zero (black in BSE images, indicative of low atomic number (low Z) elements) to 256 (white in images, indicative of high Z elements). Pixel dimensions were manually entered to match the original image scale, with an image depth (Z) value arbitrarily set to $1 \mu\text{m}$.

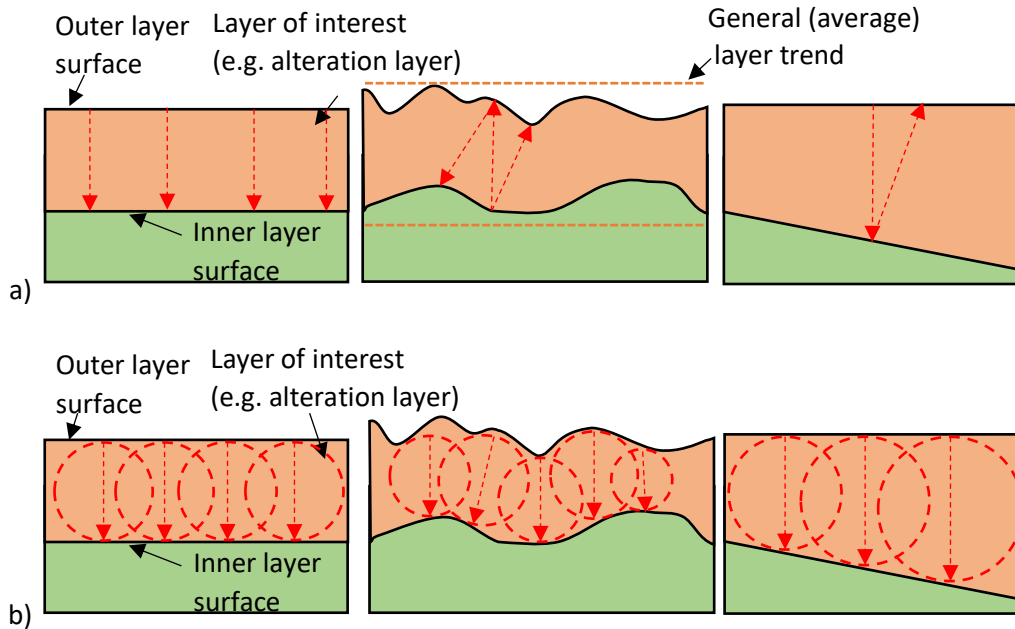


Figure 1: Comparison of methods for assessing layer thickness a) ray method with red dashed arrows indicating possible measurements of layer thickness that might be selected by different operators and b) circle method showing how the measurements are always based on the diameter of the inscribed circle

Typically the literature measures layer thickness based on straight lines, or rays, drawn between the two sides of a layer, as shown in Figure 1a this leads to ambiguities when the top and bottom surfaces of the layer are not parallel as different operators could choose different rays to characterise the layer thickness [33]. In this work layer thickness on a 2D image was measured using inscribed circles (Figure 1b), which resolves many of these ambiguities hence returning consistent results regardless of operator. This method defines the thickness at a point as the diameter of the maximum inscribed sphere contacting both surfaces of the layer. Ambiguity concerning ray orientations is removed because a circle (or sphere in 3D) will have an equal diameter in all directions; for full details see Mansfield [34].

3 Results

3.1 Chemical and physical analysis

Table 1 shows that, although there is consistency between the fixed components of the different glasses, the as-produced glasses had silica and soda molar fractions that were higher than batched, whereas alumina, lithia and magnesia molar fractions were lower than batched. The $\frac{[\text{MgO}]}{[\text{MgO}] + [\text{CaO}]}$

molar ratio achieved was generally lower than batched, however it still covers a range 0 to 0.985. The compositional results reflect evaporative losses during melting and impurities in the raw materials; for example, although only present in small amounts, SrO is consistently 50% higher than batched suggesting the presence of a Sr impurity in one of the other batched chemicals. The glasses were all predominantly X-ray amorphous prior to dissolution, although the XRD trace for the 2Ca98Mg glass indicates the presence of a small amount of a partially-crystalline component (see Figure 2a). No definitive identification of the crystalline phase could be made; however, the data is compatible with the presence of pyroxene-type mineral similar to diopside, in this glass. The Raman spectra for the two glasses with the highest Mg content, 2Ca98Mg and 33Ca67Mg, include a strong peak centred at

~ 670 cm⁻¹ (see Figure 2b) that has previously been observed in glasses with diopside (CaMgSi₂O₆) [35] and akermanite (Ca₂MgSi₂O₇) [36] compositions and where it has been associated with symmetric stretching of T-O-T bonds (T = Si or Al) in Si₂O₇ dimers [36, 37]. The low frequency feature at ~ 320 cm⁻¹ in these two glasses has been associated with lattice vibrations in akermanite [37]. The high frequency band between ~ 850 and ~ 1150 cm⁻¹, associated with Si-O⁻ stretching in SiO₄ units (see, for example, [38]), is depressed in 2Ca98Mg and 33Ca67Mg compared to the other glasses studied (see Figure 2b), however detailed inspection indicates the shape of this band is very similar for all of the glasses suggesting similar Q speciation in all cases. Density decreased linearly with increased $\frac{[\text{MgO}]}{[\text{MgO}] + [\text{CaO}]}$ from 2.758 × 10³ kg m⁻³ for 100Ca0Mg to 2.600 × 10³ kg m⁻³ for 2Ca98Mg glass.

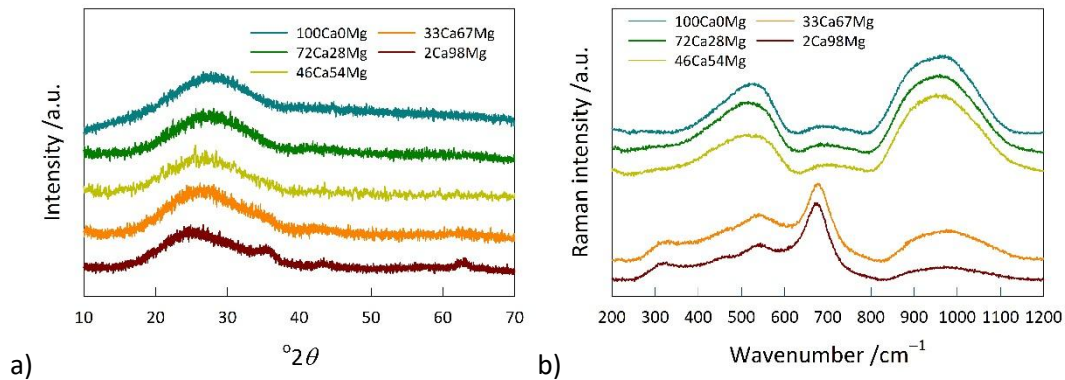


Figure 2: a) Powder X-ray diffraction and b) Raman spectra for the 5 basaltic glass compositions

3.2 Leachate analysis

Figure 3a shows that leachate pH values for the MCC-1 experiment are high (pH 9.0 to 9.5) for the first 28 – 56 d, before falling modestly (to pH 8.5 to 9) for the remainder of the experiment. Up to 224 d the 100Ca0Mg and 2Ca98Mg leachates have the highest and lowest mean pH values respectively implying a negative correlation between leachate pH over this time period and the magnesia content of the original glass. However, the 46Ca54Mg leachate exhibits the lowest pH value at 468 d and the highest pH value at 672 d. The two 1800 d samples (2Ca98Mg and 100Ca0Mg) had very significant solution losses of the order of 67 %, although in both cases the samples did remain covered by solution the SA/V value did increase to ~ 30 m⁻¹ by the end of the test. Despite the large solution losses for both of these samples the solution pH values at 1800 d of ~ pH 8.7 were similar to those at 672 d, suggesting that the endpoint glasses have similar natural pH values. Figure 3b similarly shows that the pH of the PCT-B leachates are high (pH 8.5 – 9.5) for the first 14 days falling to lower (pH 8 - 8.5) values from 14 to 112 d. Leachate pH then increases to 8.5 – 9 by 224 d. No consistent dependence of leachant pH with magnesium/calcium ratio is evident in the PCT data.

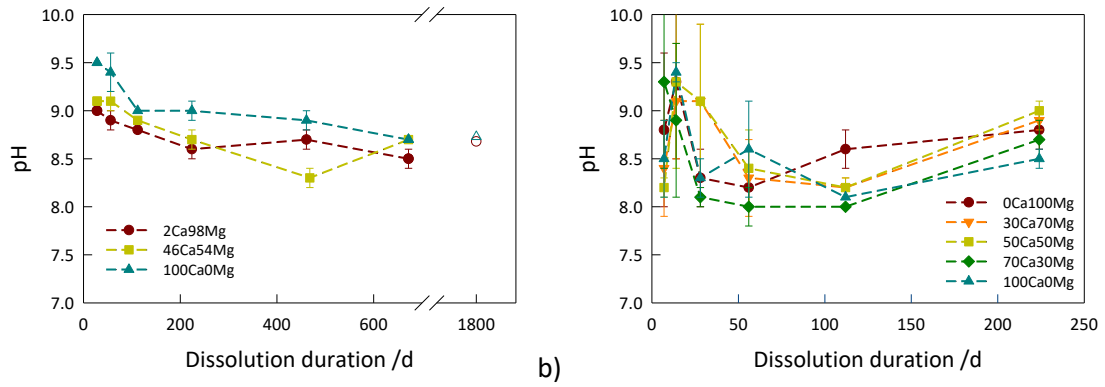
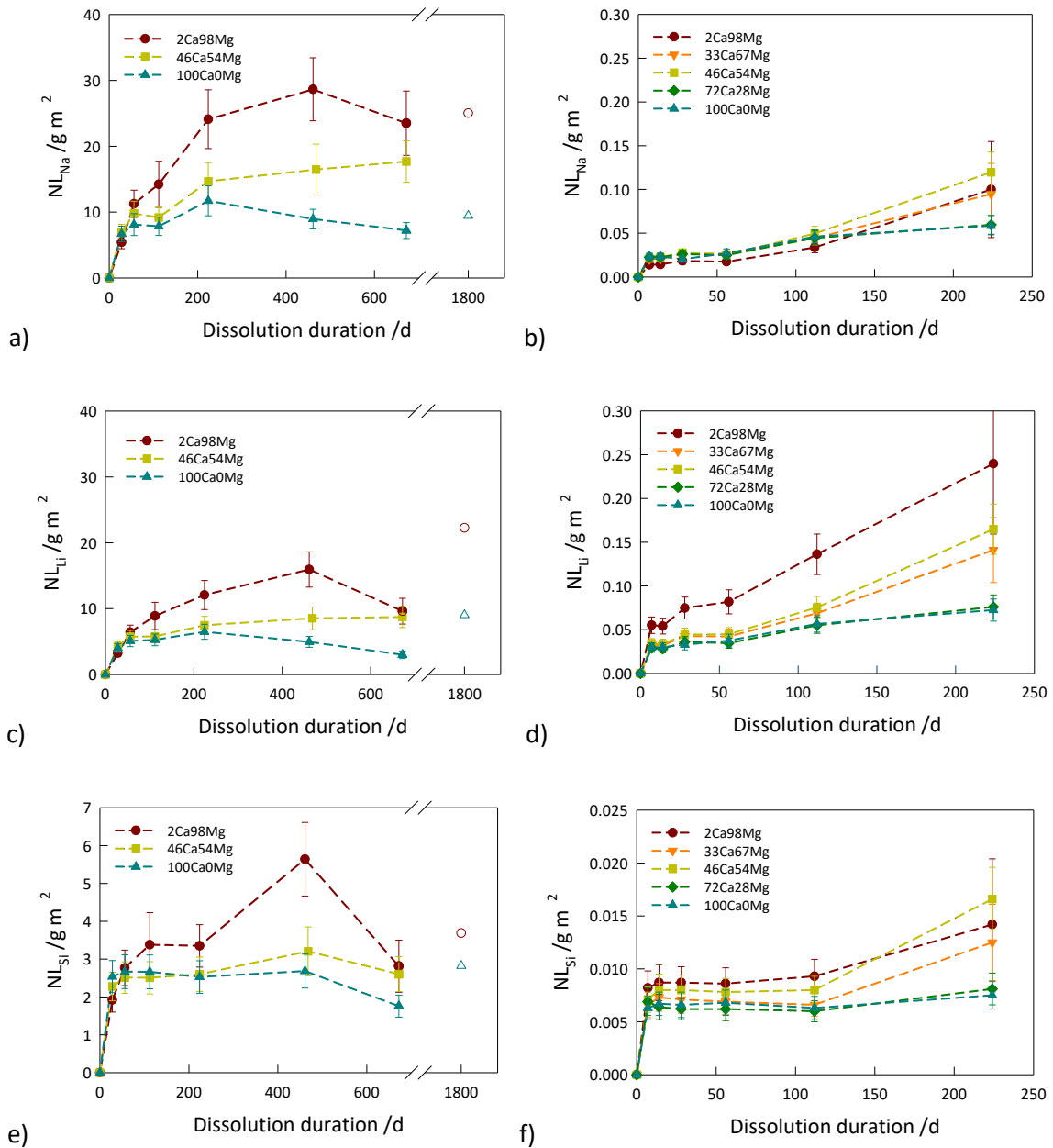


Figure 3: Solution pH and normalised losses for Na, Li, Si and Al versus time for a) MCC-1 and b) PCT-B. Lines drawn to guide the eye. Error bars are \pm one standard deviation of the triplicate samples. NB: the 1800 d MCC-1 data are both for single samples.



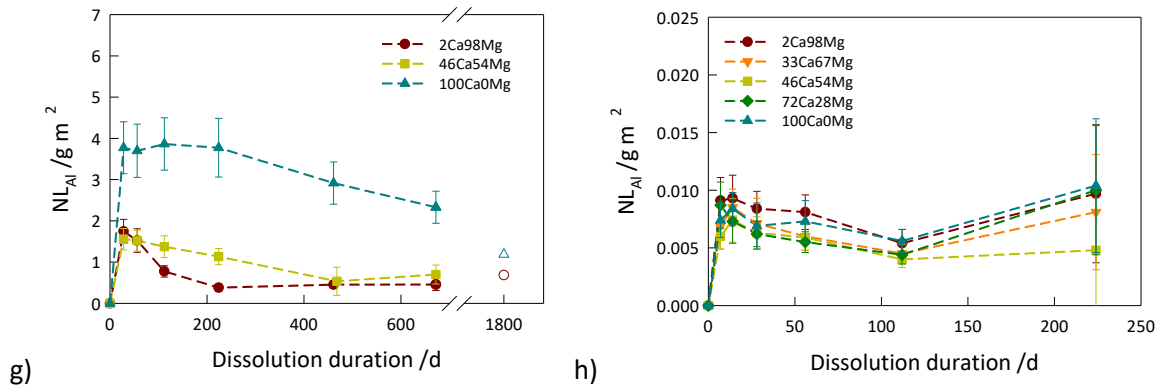


Figure 4: Normalised losses for Na, Li, Si and Al versus time for MCC-1 (a, c, e, g; left-hand side of figure) and PCT-B (b, d, f, h; right-hand side of figure). Lines drawn to guide the eye. Error bars are \pm one standard deviation of the triplicate samples. NB: the 1800 d MCC-1 data are both for single samples.

Normalised mass loss (NL_i) values for Na, Li, Si and Al from MCC-1 and PCT-B are shown in Figure 4 (parts a, c, e, g for MCC-1 and parts b, d, f, h for PCT-B respectively). For MCC-1 normalised losses of Na, Li and Si generally increase up to 468 d for 2Ca98Mg, 33Ca67Mg and 224 d for 100Ca0Mg, after which there is a decrease to 672 d. The two 1800 d samples, however, suggest that the normalised loss values, which have been corrected for solution loss, subsequently increase again for Li and Si; the Na data are less clear. For Na, Li and Si the 2Ca98Mg glass consistently shows the largest normalised mass losses and 100Ca0Mg glass the lowest. In comparison, the normalised mass loss of Al tends to decrease after 28 d for all glasses, with some indication of a small increase at longer times for the higher Mg glasses. The 100Ca0Mg glass has the largest NL_{Al} values throughout. For PCT-B NL_{Li}, NL_{Na} and NL_{Si} values are roughly constant up to 56 d and then increase approximately linearly with time for the remainder of the test duration. Again, after an initial rise the NL_{Al} values tend to decrease with time until the very final timepoint when the values increase again. For NL_{Li} the rate of this increase appears to be compositionally-dependent, with high/mid magnesium compositions (2Ca98Mg, 33Ca67Mg, 46Ca54Mg) showing the largest rate of increase. These compositions also consistently show higher NL_{Na} and NL_{Si} values than the lower magnesium glasses (72Ca28Mg, 100Ca0Mg) at any given time point. Although the pattern is not entirely consistent, these results suggest that the calcium-rich basaltic glasses are more durable than the magnesium-rich ones.

3.3 Alteration layers

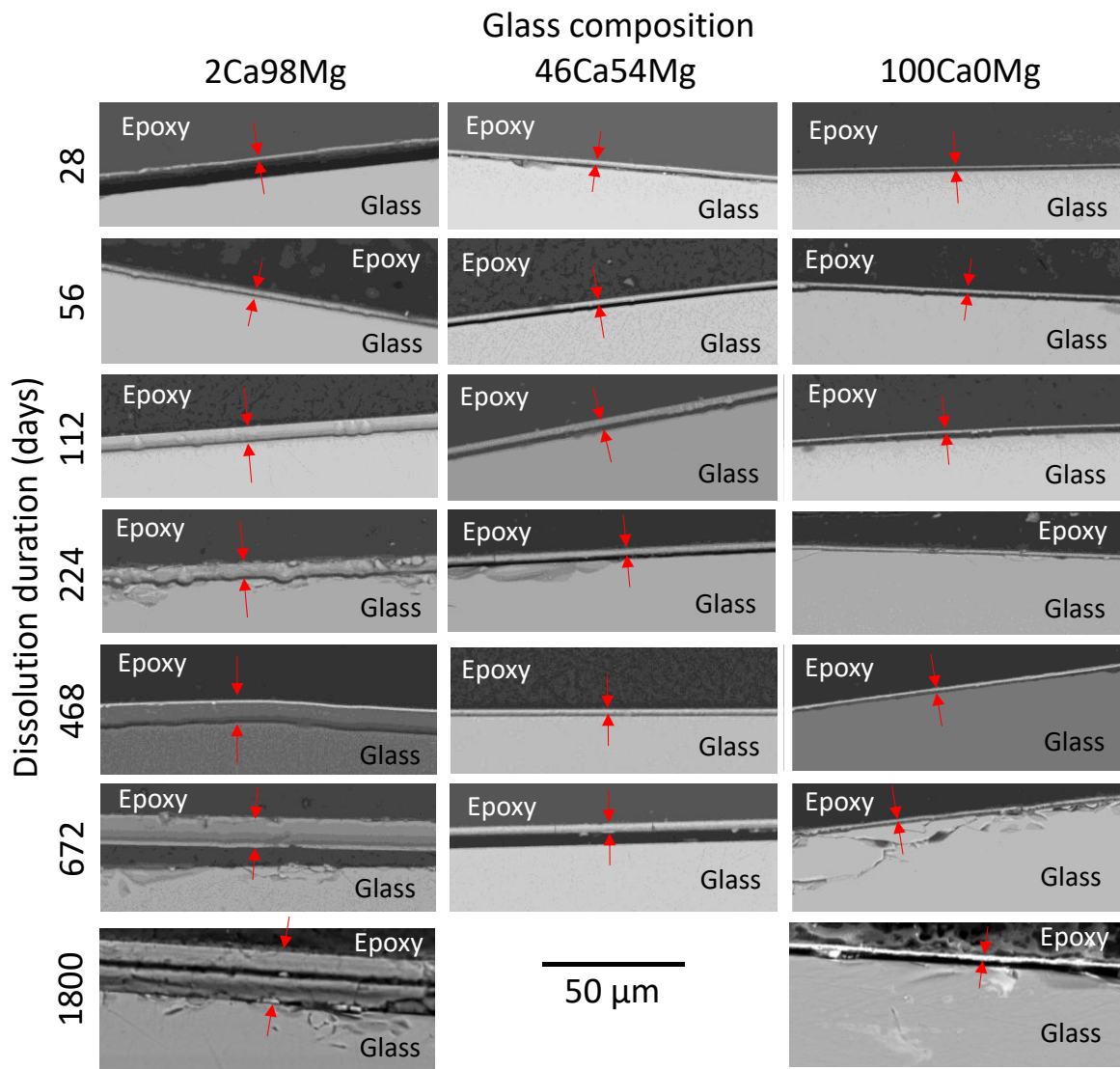


Figure 5: Representative cross-sections from the MCC-1 tests for all samples. In all cases the pristine glass is oriented towards the bottom of the image; the dark band at the top of each image is epoxy resin. The alteration layer is indicated by the red arrows; the dark gap seen between the alteration layer and the sample is considered to be an experimental artefact caused by detachment of the alteration layer from the glass surface during mounting.

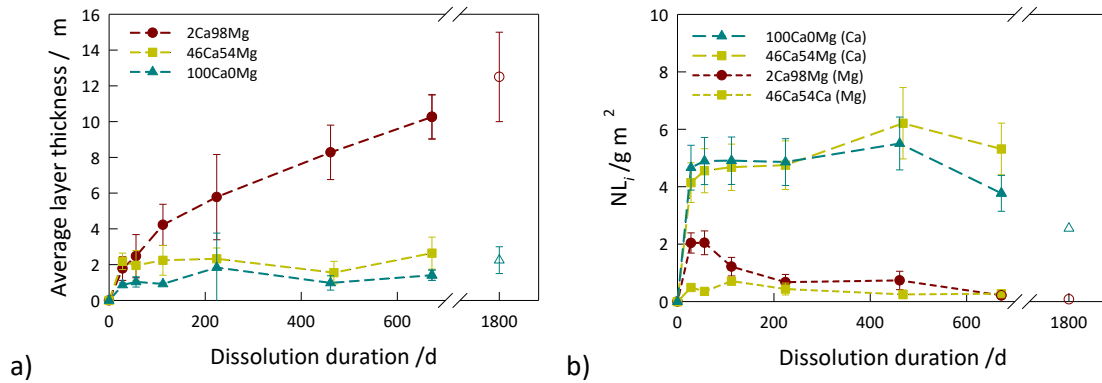


Figure 6: a) Average alteration layer thickness versus dissolution duration for the MCC-1 samples and b) the corresponding normalised loss data for Mg and Ca; lines drawn as a guide to the eye. NB: the 1800 d points are both for single samples.

Figure 5 shows representative BSE images from each basaltic glass composition at each MCC-1 time step. In all cases a heterogeneous surface layer of variable thickness and composition can be seen; this layer was found to vary considerably even across an individual monolith. However, the average layer thickness, as shown in Figure 6a as a function of test duration, was significantly larger for the highest magnesium glass (2Ca98Mg), with this thickness increasing to $\sim 10 \mu\text{m}$ after 672 d. The 100Ca0Mg glass consistently had the lowest layer thicknesses, with this layer remaining approximately the same thickness ($\sim 0.8 - 1.8 \mu\text{m}$) for the entire test duration. The 46Ca54Mg glass samples typically have an alteration layer with intermediate thickness; however, the thickness of this layer is closer to (and often within error of) the magnesium-free end member. The 46Ca54Mg samples also show relatively constant alteration layer thickness ($\sim 1.5 - 2.6 \mu\text{m}$) with dissolution duration (see Figure 6a). The two end member MCC-1 samples left for 1800 d confirm this trend with the alteration layer thickness on the 100Ca0Mg sample measuring $1.5 - 3 \mu\text{m}$ whilst that on the 2Ca98Mg sample measured $10 - 15 \mu\text{m}$. This implies that, after formation, further growth in thickness of the surface layer only occurs when the pristine basaltic glass contains magnesium and does not contain calcium.

After the initial time point, the NL_{Ca} data remain relatively constant (see Figure 6b) for the 46Ca54Mg and 100Ca0Mg samples, although NL_{Ca} does decrease for the 1800 d 100Ca0Mg sample. Meanwhile the NL_{Mg} for the 2Ca98Mg sample goes through a maximum between 28 and 56 d, which indicates that at times greater than 56 d Mg is being incorporated into alteration products for this glass. For the 46Ca54Mg sample the NL_{Mg} data remains low and relatively constant after the initial time point (Figure 6b) again suggesting that the Mg is being incorporated into alteration products rather than being released.

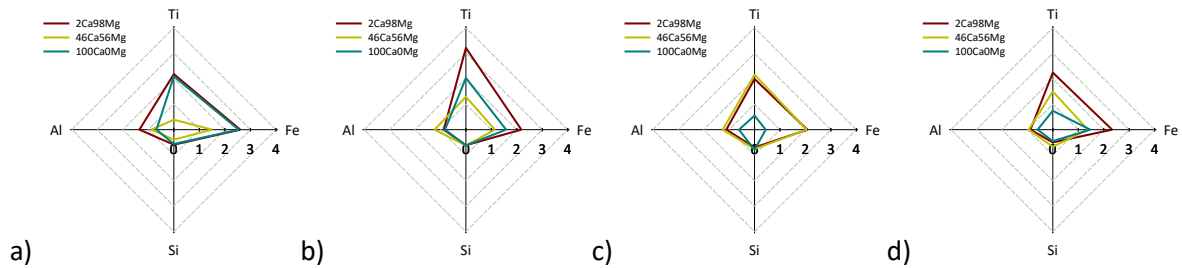


Figure 7: Normalised elemental content of the surface layers observed in the MCC-1 tests (normalised to the relevant pristine glass composition) after a) 56 d, b) 112 d, c) 461 d (468 d for Ca46Mg54), d) 672 d.

There is no clear correlation between surface layer composition and time (see Figure 7). Fe and Ti tend to be elevated compared to the initial glass, with the greatest level of enrichment being found in the 2Ca98Mg samples, and at longer times Ti is reduced in the 100Ca0Mg glass. In comparison Si tends to be depleted and Al little changed.

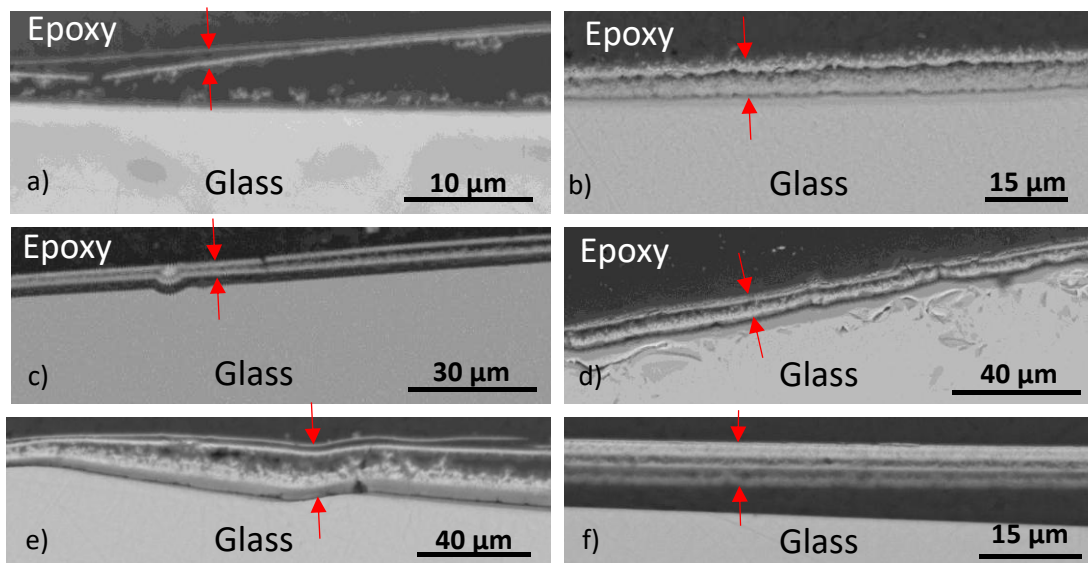


Figure 8: SEM-BSE images showing the cleaving of the surface alteration layer into sub-layers evident in 46Ca54Mg and 100Ca0Mg basaltic glasses after dissolution: a) 100Ca0Mg after 28 d; b) 46Ca54Mg after 56 d; c) 46Ca54Mg after 112 d; d) 46Ca54Mg after 224 d; e) 46Ca54Mg after 468 d and f) 46Ca54Mg after 672 d. In all cases the pristine glass is oriented towards the bottom of the image; the dark band at the top of each image is epoxy resin. The alteration layer is indicated by the red arrows; the dark gap seen between the alteration layer and the sample is considered to be an experimental artefact caused by detachment of the alteration layer from the glass surface during mounting.

The alteration layers were frequently broken, likely during sample preparation, into block-like segments by fractures that are approximately perpendicular to the surface. In places, this surface layer cleaves into sub-layers as shown in Figure 8: with two layers evident by 28 days (Figure 8a) and three layers emerging after 468 days (Figure 8e). These sub-layers are frequently separated by (a layer of) apparently fibrous material, and are evident in both 100Ca0Mg and 46Ca54Mg glasses. The epoxy-filled voids that separates the alteration layer from the pristine glass and the sub-layers from each other are presumed to arise during sample preparation and to be a result of dehydration shrinkage.

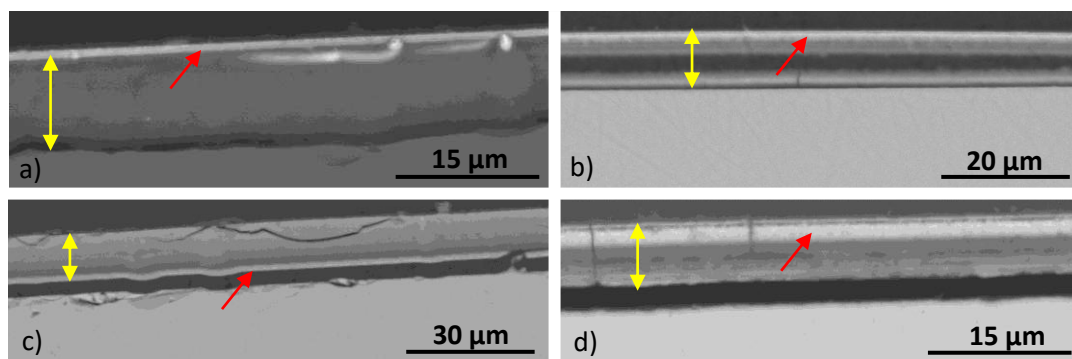


Figure 9: SEM-BSE images of 'brighter' sub-layer (arrowed in red) within the surface layer (layer depth indicated by the yellow arrow) developed on basaltic glasses: a) 2Ca98Mg after 461 d; b) 46Ca54Mg after 468 d; c) 2Ca98Mg after 672 d and d) 46Ca54Mg after 672 d.

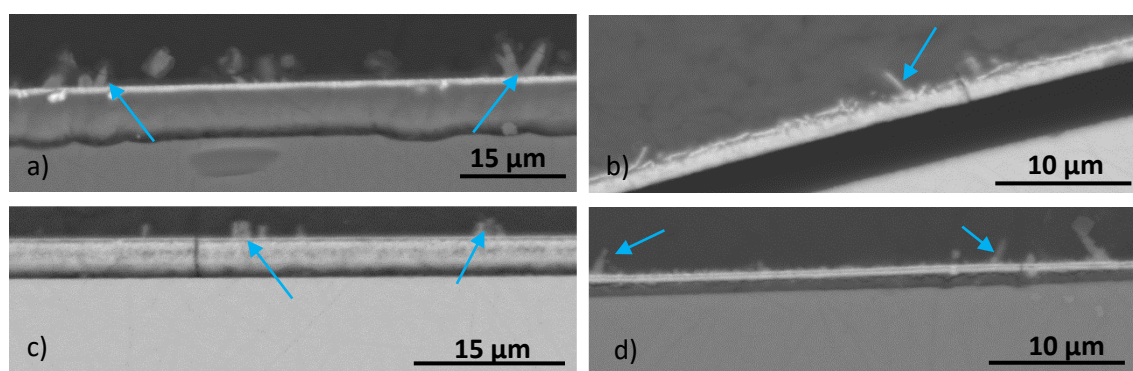


Figure 10: SEM-BSE images of precipitates (arrowed) formed on the outer surface of the alteration layer for all glass compositions after > 56 d of dissolution: a) 2Ca98Mg after 461 d; b) 46Ca54Mg after 672 d; c) 46Ca54Mg after 468 d and d) 100Ca0Mg after 461 d.

The surface layer is also highly heterogeneous in greyscale intensity as shown in Figure 8 and Figure 9 indicating compositional non-uniformities. Although the bulk surface layer is typically of similar greyscale intensity to the unaltered glass, a 'brighter' sub-layer, typically 0.5 - 2 μm in thickness, which may be located either near to the outer surface or to the pristine glass is evident (compare 2Ca98Mg after 468 d in Figure 9b and after 672 d in Figure 9c). Precipitates are seen on the outer surface of the alteration layer after 56 d for all compositions (see Figure 10), although they may be slightly more common in the high-magnesia glasses. These precipitates generally become larger and more numerous with increasing dissolution duration.

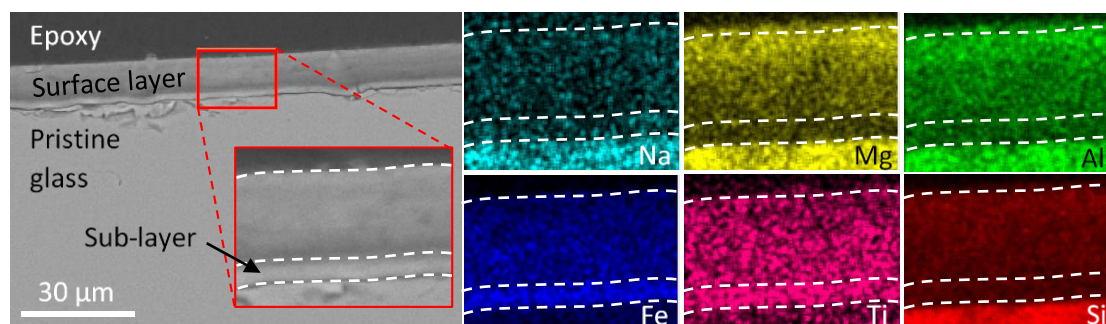


Figure 11: BSE image and corresponding EDS elemental maps of a cross-section of the surface of a 2Ca98Mg MCC-1 monolith after 672 d dissolution

Figure 11 indicates that the surface layer of a 2Ca98Mg monolith after 672 d dissolution is depleted in Na, Si, Mg and Al, although higher levels of Mg and Al are seen in the outermost regions of the layer. Increased Fe and Ti are found in the sub-layer that is adjacent to the unaltered parent glass.

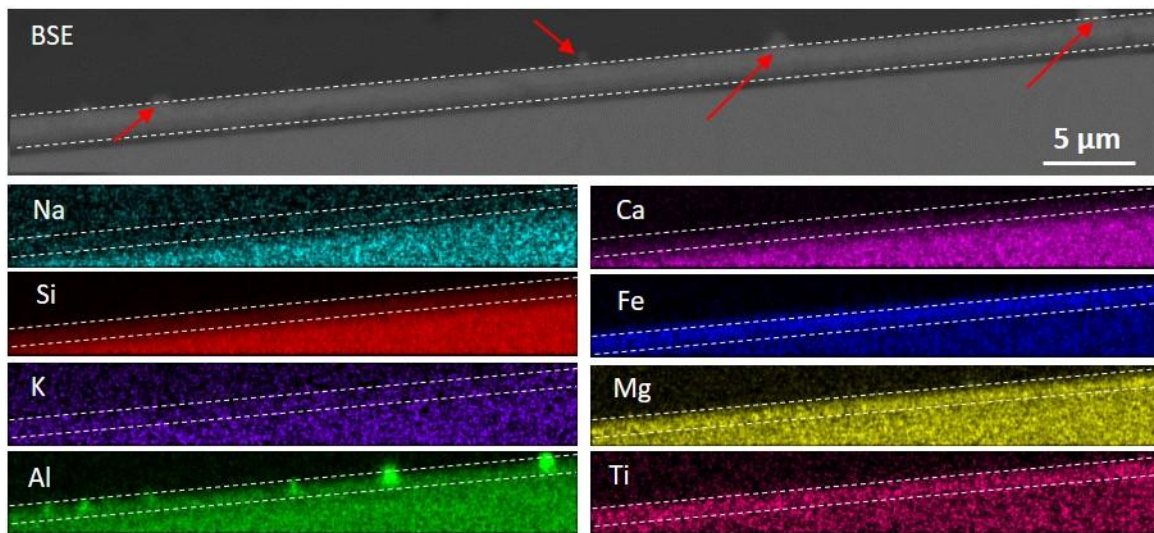


Figure 12: BSE image and corresponding EDS elemental maps of a cross-section of the surface of a 46Ca54Mg MCC-1 monolith after 112 d dissolution.

Figure 12 similarly shows that the sub-layer adjacent to the unaltered parent glass in a 46Ca54Mg sample after 112 d dissolution is somewhat enriched in iron and titanium. More detailed compositional quantification of these sub-layers was not possible owing to their slender nature and the available imaging resolution. Elemental maps of the particles on top of and partially penetrating the surface alteration layer (Figure 12) show these to be highly enriched in aluminium relative to the parent glass.

4 Discussion

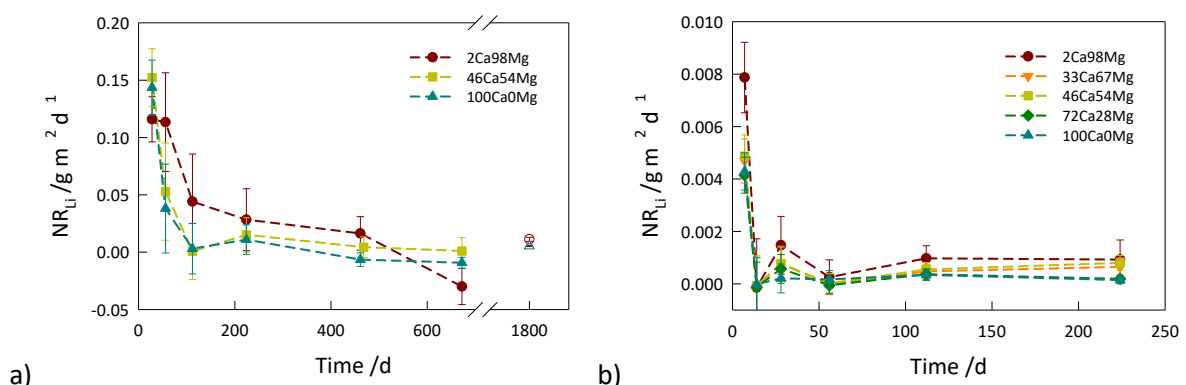


Figure 13: Normalised release rates for Li for a) MCC-1 experiments and b) PCT experiments. Rates calculated for adjacent timepoints using equation (2). Lines drawn to guide the eye. Error bars are \pm one standard deviation of the triplicate samples. NB: the 1800 d MCC-1 data are both for single samples.

Elements such as Si and Al are readily included in secondary mineral phases and, therefore, their concentration in solution will be controlled by precipitation at the glass surface; PCT tests show

reduced release rates of Si and Al compared to Li and Na, whilst MCC-1 tests show removal of Si and Al from solution over time. None of the basaltic glasses contain B, an element commonly used as a glass dissolution tracer as it does not associate with most secondary alteration minerals, and thus an alternative element has to be used. Figure 11 indicates that sodium is not significantly retained within the alteration layer. Meanwhile comparison of Figure 4a, b, c and d indicate that while the trends for NL_{Na} and NL_{Li} are similar for both MCC-1 and PCT for MCC-1 $NL_{Na} > Na_{Li}$ whereas for PCT $NL_{Li} > Na_{Na}$. It is not clear which of these two elements should be considered the more reliable, although Utton *et al.* [39] reported for the glasses they studied $NL_{Li} \sim NL_B$ and Goût *et al.* [40] indicate that Li is leached more rapidly than Na. Hence Li has been chosen here. Figure 13 shows the normalised release rates for Li for both the MCC-1 and PCT experiments calculated using

$$NR_{Li} = \frac{\Delta NL_{Li}}{\Delta t} \quad (2)$$

where ΔNL_{Li} is the difference in normalised losses of Li and Δt is the time increment for two adjacent time points. It can be seen from Figure 13 that the normalised release rates tend to decrease with decreasing Mg and increasing Ca in the glass. In all cases there are relatively high initial release rates (Figure 13), which result in the initial rapid increase in pH values (Figure 3a and b) as appreciable alkali/alkaline earth ions are released into solution. Subsequently the normalised release rates decrease. Figure 13b indicates that the normalised release rates for Li are roughly constant for all glasses after 28 d for the PCT experiment. Similarly Figure 13a indicates that Li release rates measured in MCC-1 are relatively constant from 224 to 620 d for the 2 glasses containing larger amounts of Ca (46Ca54Mg and 100Ca0Mg) whereas for the highest Mg sample NL_{Li} goes negative suggesting that some Li is removed from solution (this is also the case for the Na normalised release rates). In comparison the two 1800 d MCC-1 samples suggest there may be an increase in the normalised release rate for both 2Ca98Mg and 100Ca0Mg at longer times. Overall there is no strong evidence for significant rate resumption in these experiments although detachment of alteration layers/sublayers may have resulted in the exposure of fresh glass surface to solution and a corresponding temporary higher release rates until new layers are formed.

In terms of absolute values, the normalised release rates for PCT-B are typically two orders of magnitude lower than the rates calculated for MCC-1 experiments reflecting the different stages of dissolution that these experiments interrogate. Further discrepancy may result from the 50 °C temperature used for the PCT-B experiments as compared to the 90 °C used for the MCC-1 experiments.

The observed positive correlation between magnesium content and dissolution rates, and negative correlation between calcium concentration and dissolution rates, may have several contributing explanations. Firstly, the passivating effect of calcium on glass alteration has been previously observed (see [41, 42] and references therein), with Mercado-Depierre *et al.* noting that “at near-neutral pH and high reaction progress, a Si-Ca rich passivating layer forms at the glass surface and is significantly enhanced by the presence of low soluble cross-linking elements in the glass such as Al” as is the case in these experiments. This could be the origin of the fibrous material in the alteration layers shown in Figure 8. Secondly features evident in the XRD data for the highest Mg content glasses (Figure 2a; 2Ca98Mg only) and the Raman data (Figure 2b; 2Ca98Mg and 33Ca67Mg) suggest that regions of reduced connectivity may be present in these glasses that are not present in the higher Ca content glasses. Less well connected regions are likely to show increased propensity for chemical attack. Thirdly, increased rates of dissolution in Mg containing glasses may result from an increased

propensity for mineral precipitation from solutions into which magnesium has leached [10, 12, 24] or is otherwise present [43-45]. The magnesium aluminate, meixnerite [20, 46] and aluminous hectorites have been identified as minerals likely to precipitate with increasing magnesium contents [12]. Hectorite is also often observed as secondary alteration product of (crystalline) basaltic lava flows [47]. The NL_{Al} data (see Figure 4i) are lower and decrease more rapidly for high-magnesium basaltic glasses and this, coupled with low NL_{Mg} values (see Figure 6b), imply that aluminium and magnesium are consumed from the solution, likely forming precipitates. Thien *et al.* [12] give the formula of aluminous hectorite as $Na_{0.52}(Mg_{2.47}Li_{0.12}Al_{0.11}Fe_{0.01}M_{0.29})(Si_{3.45}Al_{0.55})O_{10}(OH)_2$, where M = trace cation. This is compatible with the observation of elevated levels of aluminium in the particles shown in Figure 12. In addition, during sampling, a translucent, white/cream foliated material with an earthy to waxy lustre was observed at the waterline of vessels containing 2Ca98Mg basaltic glass. This material conforms to the mineralogical description of hectorite [48], but was not present in sufficient quantities and was too delicate to allow XRD or further analysis. Although in principle geochemical modelling could possibly provide support for the formation of this mineral, the solubility product and other relevant data for hectorite is absent from many thermodynamic databases [49].

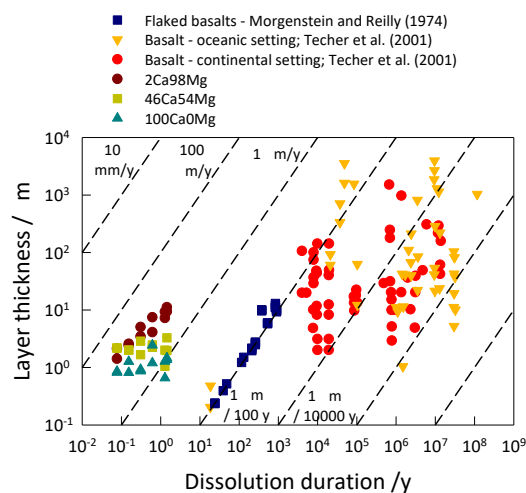


Figure 14: Comparison of measured layer thicknesses with literature data for natural and worked basaltic glasses; data drawn from [3, 50]

The data shown in Figure 6a are compared in Figure 14 to literature data for natural basaltic glasses from both continental and oceanic settings (data taken from [3], which drew on a range of original sources), and some worked basalts from archaeological contexts [50]. Also shown are lines of constant alteration rates. In agreement with other data, rates tend to be lowest for the highest Ca content glass (100Ca0Mg). The alteration rates for the laboratory samples ($\geq 1 \mu\text{m}/\text{y}$) are generally at least 2 orders of magnitude greater than the reported rates ($\leq 1 \mu\text{m}/100 \text{y}$) for natural basalts found in either continental or oceanic settings or the flaked basalts found in archaeological settings. This likely reflects the elevated temperatures (90 °C for the MCC-1 tests) which are regularly used in laboratory tests compared to those found in the natural environment.

The spread of alteration layer thicknesses developed on natural basalts will reflect a number of variables. These include differences in leaching conditions, variations in leachate chemistries [51], and the significant uncertainty in dissolution duration of many of the natural basaltic glasses reported by the original authors [31]. This is because aqueous exposure duration does not necessarily equate to sample age [52] and also an unknown thickness of alteration layer may have been removed over time depending on the environment surrounding the glass. Additionally, as also seen in the laboratory data

reported here, the reported alteration layer thicknesses can vary considerably across a single sample surface [31]. All of this may indicate that alteration rates on natural basalts in continental or oceanic settings are higher than those indicated by Figure 14. Although the flaked basalts reported by Morgenstein & Riley [50] apparently have a very consistent alteration rate, comparable with the highest rates reported on natural basalts, this is a direct consequence of their assessment methodology and thus their results need to be treated with some caution. Despite these caveats about alteration rates in natural basalts the scale of the difference between the current laboratory data and the natural basalt data does suggest that the laboratory tests are giving accelerated rates, which is to be expected given the elevated temperatures utilised (90 °C for the MCC-1 tests) and indicates that the normalised release rates shown in Figure 13 are also accelerated values.

5 Conclusions

For the series of synthetic basaltic glasses, temperatures and times studied, magnesium-rich compositions generally have a lower durability than the calcium rich ones whether this is assessed by normalised loss values, normalised release rates or alteration layer thicknesses. Typically, in the alteration layers, a set of sub-layers can be identified, however the significant feature is the reduced Al and Mg contents of the main layer in the magnesium rich compositions. It is likely that Al and Mg are instead being used to form the observed secondary precipitates, potentially including aluminous hectorites, and which appear to form more readily on higher-magnesium glasses. Despite the apparent consumption of Mg there is only limited evidence of rate resumption for these glasses.

The laboratory assessed alteration rates based on alteration layer thicknesses from the MCC-1 tests at 90 °C are demonstrated to be at least 2 orders of magnitude greater than the alteration rates reported on natural basalts in a range of ambient continental and oceanic settings.

6 Acknowledgements

James Mansfield thanks the UK Engineering and Physical Sciences Research Council (EPSRC) and the United Kingdom National Nuclear Laboratory (UKNNL) for funding as part of the Next Generation Nuclear (NGN) Centre for Doctoral Training programme. We thank Lisa Hollands and Tes Monaghan (both University of Sheffield) for help with glass melting and sample preparation respectively. We thank the University of Sheffield's Faculty of Science Mass Spectrometry Centre for the HF digest ICP-OES measurements. Claire Corkhill acknowledges EPSRC for the award of an Early Career Research Fellowship (EP/N017374/1). Clare Thorpe acknowledges EPSRC for the award of a David Clarke Fellowship (EP/S012400/1) and the Royal Society for the award of a Dorothy Hodgkin Fellowship. This research utilised the HADES/MIDAS facility [53] at the University of Sheffield established with financial support from EPSRC and BEIS, under grant EP/T011424/1, and the PLEIADES facility, established with financial support from the EPSRC National Nuclear User Facility (EP/V035215/1).

7 References

- [1] G. Malow, W. Lutze, and R. C. Ewing, "Alteration effects and leach rates of basaltic glasses: implications for the long-term stability of nuclear waste form borosilicate glasses," *Journal of Non-Crystalline Solids*, vol. 57, pp. 305-321, 1984, doi: 10.1016/0022-3093(84)90156-X.
- [2] J. L. Crovisier, J. Honnorez, and J. P. Eberhart, "Dissolution of basaltic glasses in seawater: mechanism and rate," *Geochimica et Cosmochimica Acta*, vol. 51, pp. 2977-2990, 1987, doi: 10.1016/0016-7037(87)90371-1.
- [3] I. Techer, J. Lancelot, N. Clauer, J. M. Liotard, and T. Advocat, "Alteration of a basaltic glass in an argillaceous medium: The Salagou dike of the Lode`ve Permian Basin (France). Analogy

- with an underground nuclear waste repository," *Geochimica et Cosmochimica Acta*, vol. 65, pp. 1071-1086, 2001, doi: 10.1016/S0016-7037(00)00583-4.
- [4] R. C. Ewing and R. F. Haaker, "Naturally occurring glasses: analogues for radioactive waste forms," PNL-2776; Pacific Northwest Laboratory, 1979. [Online]. Available: <https://www.osti.gov/biblio/5993747>
- [5] M. J. Jercinovic and R. C. Ewing, "Basaltic glasses from Iceland and the deep sea: natural analogues to borosilicate nuclear waste-form glass," University of New Mexico, Albuquerque, 1987. [Online]. Available: https://inis.iaea.org/search/search.aspx?orig_q=RN:20042698
- [6] I. Techer, T. Advocat, J. Lancelot, and J.-M. Liotard, "Basaltic glass: alteration mechanisms and analogy with nuclear waste glasses," *Journal of Nuclear Materials*, vol. 282, pp. 40-46, 2000, doi: 10.1016/S0022-3115(00)00399-8.
- [7] M. T. Harrison, "Vitrification of high level waste in the UK," *Procedia Materials Science*, pp. 10-15, 2014, doi: 10.1016/j.mspro.2014.10.003.
- [8] R. Short, "Phase separation and crystallisation in UK HLW vitrified products," *Procedia Materials Science*, vol. 7, pp. 93-100, 2014, doi: 10.1016/j.mspro.2014.10.013.
- [9] I. W. Donald, B. L. Metcalfe, and R. N. J. Taylor, "The immobilization of high level radioactive wastes using ceramics and glasses," *Journal of Materials Science*, vol. 1997, pp. 5851-5887, 1997, doi: 10.1023/A:1018646507438.
- [10] P. Frugier, C. Martin, I. Ribet, T. Advocat, and S. Gin "The effect of composition on the leaching of three nuclear waste glasses: R7T7, AVM and VRZ," *Journal of Nuclear Materials*, vol. 346, pp. 194-207, 2005, doi: 10.1016/j.jnucmat.2005.06.023.
- [11] B. Thien, N. Godon, F. Hubert, F. Angeli, S. Gin, and A. Ayrat, "Structural identification of a trioctahedral smectite formed by the aqueous alteration of a nuclear glass," *Applied Clay Science*, vol. 49, pp. 135-141, 2010, doi: 10.1016/j.clay.2010.04.016.
- [12] B. M. J. Thien, N. Godon, A. Ballesterro, S. Gin, and A. Ayrat, "The dual effect of Mg on the long-term alteration rate of AVM nuclear waste glasses," *Journal of Nuclear Materials*, vol. 427, pp. 297-310, 2012, doi: 10.1016/j.jnucmat.2012.05.025.
- [13] P. Frugier *et al.*, "SON68 nuclear glass dissolution kinetics: Current state of knowledge and basis of the new GRAAL model," *Journal of Nuclear Materials*, vol. 380, pp. 8-21, 2008, doi: 10.1016/j.jnucmat.2008.06.044.
- [14] R. H. Doremus, Y. Mehrotra, W. A. Lanford, and C. Burman, "Reaction of water with glass: influence of a transformed surface layer," *Journal of Materials Science*, vol. 18, pp. 612-622, 1983, doi: 10.1016/B978-0-7204-0419-7.50017-2.
- [15] C. L. Thorpe, "Forty years of durability assessment of nuclear waste glass by standard methods," *npj Materials Degradation*, vol. 5, p. 61, 2021, doi: 10.1038/s41529-021-00210-4.
- [16] B. Grambow and R. Mueller, "First-order dissolution rate law and the role of surface layers in glass performance assessment," *Journal of Nuclear Materials*, vol. 298, pp. 112-124, 2001, doi: 10.1016/S0022-3115(01)00619-5.
- [17] C. Lenting, O. Pluemper, M. Kilburn, P. Guagliardo, M. Klinkenberg, and T. Geisler, "Towards a unifying mechanistic model for silicate glass corrosion," *npj Materials Degradation*, vol. 2, p. 28, 2018, doi: 10.1038/s41529-018-0048-z.
- [18] T. Geisler, A. Janssen, D. Scheiter, T. Stephan, J. Berndt, and A. Putnis, "Aqueous corrosion of borosilicate glass under acidic conditions: A new corrosion mechanism," *Journal of Non-Crystalline Solids*, vol. 356, pp. 1458-1465, 2010, doi: 10.1016/j.jnoncrysol.2010.04.033.
- [19] R. Hellmann *et al.*, "Nanometre-scale evidence for interfacial dissolution–reprecipitation control of silicate glass corrosion," *Nature Materials*, vol. 14, pp. 307-311, 2015, doi: 10.1038/nmat4172.
- [20] D. J. Backhouse, "A study of the dissolution of nuclear waste glasses in highly-alkaline conditions," PhD, University of Sheffield, 2017. [Online]. Available: <https://etheses.whiterose.ac.uk/16760/>

- [21] S. Gin *et al.*, "Nuclear glass durability: new insight into alteration layer properties," *Journal of Physical Chemistry C*, vol. 115, pp. 18696-18706, 2011, doi: 10.1021/jp205477q.
- [22] M. Fournier, P. Frugier, and S. Gin, "Resumption of alteration at high temperature and pH: rates measurements and comparison with initial rates," *Procedia Materials Science*, vol. 7, pp. 202-208, 2014, doi: 10.1016/j.mspro.2014.10.026.
- [23] N. Bisbrouck, M. Micoulaut, J. M. Delaye, S. Gin, and F. Angeli, "Structure-property relationship and chemical durability of magnesium-containing borosilicate glasses with insight from topological constraints," *npj Materials Degradation*, vol. 6, 2022, doi: 10.1038/s41529-022-00268-8.
- [24] E. Curti, J. L. Crovisier, G. Morvan, and A. M. Karpoff, "Long-term corrosion of two nuclear waste reference glasses (MW and SON68): A kinetic and mineral alteration study," *Applied Geochemistry*, vol. 21, pp. 1152-1168, 2006, doi: 10.1016/j.apgeochem.2006.03.010.
- [25] D. J. Backhouse, C. L. Corkhill, N. C. Hyatt, and R. J. Hand, "Investigation of the role of Mg and Ca in the structure and durability of aluminoborosilicate glass," *Journal of Non-Crystalline Solids*, vol. 512, pp. 41-52, 2019, doi: 10.1016/j.jnoncrysol.2019.03.003
- [26] A. J. Fisher, M. T. Harrison, N. C. Hyatt, R. J. Hand, and C. L. Corkhill, "The dissolution of simulant UK Ca/Zn-modified nuclear waste glass: Insight into Stage III behaviour " *MRS Advances*, vol. 5, pp. 103-109, 2020, doi: 10.1557/adv.2020.50
- [27] C. D. Byers, M. J. Jercinovic, and R. C. Ewing, "A study of natural glass analogues as applied to alteration of nuclear waste glass," Argonne National Laboratory, Argonne, 1987.
- [28] J. T. Mansfield, C. L. Thorpe, C. L. Corkhill, M. T. Harrison, and R. J. Hand, "Localised extended ("vermiform") features formed during glass dissolution," *Journal of Non-Crystalline Solids*, vol. 608, 2023, doi: 10.1016/j.jnoncrysol.2023.122230.
- [29] *C1220-17 Standard test method for static leaching of monolithic waste forms for disposal of radioactive waste*, ASTM, 2017. [Online]. Available: <https://www.astm.org/standards/c1220>
- [30] *C1285-21 Standard test methods for determining chemical durability of nuclear, hazardous, and mixed waste glasses and multiphase glass ceramics: the product consistency test (PCT)*, ASTM, 2021. [Online]. Available: <https://www.astm.org/standards/c1285>
- [31] I. Techer, T. Advocat, J. Lancelot, and J. M. Liotard, "Dissolution kinetics of basaltic glasses: control by solution chemistry and protective effect of the alteration film," *Chemical Geology*, vol. 176, pp. 235-263, 2001, doi: 10.1016/S0009-2541(00)00400-9.
- [32] *Dragonfly 2022.2 [Computer software]*. Comet Technologies Canada Inc. , Montreal, Canada. [Online]. Available: <https://www.theobjects.com/dragonfly>
- [33] M. Inui, N. Umezumi, K. Wakasaki, and S. Sato, "Thickness and clearance visualization based on distance field of 3D objects," *Journal of Computer Design Engineering*, vol. 2, pp. 183-194, 2015, doi: 10.1016/j.jcde.2015.04.001.
- [34] J. T. Mansfield, "Aqueous dissolution of nuclear waste and analogue glasses: dissolution behaviour, surface layers and vermiform features," University of Sheffield, 2022. [Online]. Available: <https://etheses.whiterose.ac.uk/31900/>
- [35] J. Etchepare, "Study by Raman spectroscopy of crystalline and glassy diopside," in *Amorphous Materials*, R. W. Douglas and B. Ellis Eds. London: Wiley-Interscience, 1972, pp. 337-346.
- [36] S. K. Sharma, H. S. Yoder, and D. W. Matson, "Raman study of some melilites in crystalline and glassy states," *Geochimica et Cosmochimica Acta*, vol. 52, pp. 1961-1967, 1988, doi: 10.1016/0016-7037(88)90177-9.
- [37] A. R. Allu *et al.*, "Structure and crystallization of alkaline-earth aluminosilicate glasses: prevention of the alumina-avoidance principle," *Journal of Physical Chemistry B*, vol. 122, pp. 4737-4747, 2018, doi: 10.1021/acs.jpcc.8b01811.
- [38] C. Le Losq, M. R. Cicconi, G. N. Greaves, and N. D. R., "Silicate Glasses," in *Springer Handbook of Glass*, J. D. Musgraves, J. Hu, and L. Calvez Eds. Cham: Springer, 2019, ch. 13, pp. 441-504.

- [39] C. A. Utton, R. J. Hand, P. A. Bingham, N. C. Hyatt, S. W. Swanton, and S. J. Williams, "Dissolution of vitrified wastes in a high-pH calcium-rich solution," *Journal of Nuclear Materials*, vol. 435, pp. 112-122, 2013, doi: 10.1016/j.jnucmat.2012.12.032.
- [40] T. L. Gout, M. T. Harrison, and I. Farnan, "Impacts of lithium on Magnox waste glass dissolution," *Journal of Non-Crystalline Solids*, vol. 517, pp. 96-105, 2019, doi: 10.1016/j.jnoncrysol.2019.04.040.
- [41] S. Mercado-Depierre, F. Angeli, F. Frizon, and S. Gin, "Antagonist effects of calcium on borosilicate glass alteration," *Journal of Nuclear Materials*, vol. 441, pp. 402-410, 2013, doi: 10.1016/j.jnucmat.2013.06.023.
- [42] C. L. Corkhill, N. J. Cassingham, P. G. Heath, and N. C. Hyatt, "Dissolution of UK High-Level Waste Glass Under Simulated Hyperalkaline Conditions of a Colocated Geological Disposal Facility," *International journal of Applied Glass Science*, vol. 4, pp. 341-356, 2013, doi: 10.1111/ijag.12042.
- [43] A. Arena *et al.*, "Impact of Zn, Mg, Ni and Co elements on glass alteration: Additive effects," *Journal of Nuclear Materials*, vol. 470, pp. 55-67, 2016, doi: 10.1016/j.jnucmat.2015.11.050.
- [44] A. Arena *et al.*, "Impact of iron and magnesium on glass alteration: Characterization of the secondary phases and determination of their solubility constants," *Applied Geochemistry*, vol. 82, pp. 119-133, 2017, doi: 10.1016/j.apgeochem.2017.04.010.
- [45] A. Arena *et al.*, "Impact of Fe, Mg and Ca elements on glass alteration: Interconnected processes" *Geochimica et Cosmochimica Acta*, vol. 239, pp. 420-445, 2018, doi: 10.1016/j.gca.2018.08.007.
- [46] C. L. Corkhill *et al.*, "Surface interfacial analysis of simulant high level nuclear waste glass dissolved in synthetic cement solutions," *npj Materials Degradation*, vol. 6, 2022, doi: 10.1038/s41529-022-00279-5.
- [47] W. F. Foshag and A. O. Woodford, "Bentonitic magnesian clay-mineral from California," *American Mineralogist*, vol. 21, pp. 238-244, 1936.
- [48] J. W. Anthony, R. A. Bideaux, K. W. Bladh, and M. C. Nichols, Eds. *Handbook of Mineralogy*. Chantilly, Virginia: Mineralogical Society of America, 2001. [Online]. Available: <http://www.handbookofmineralogy.org/>.
- [49] M. Debure, P. Frugier, L. De Windt, and S. Gin "Borosilicate glass alteration driven by magnesium carbonates," *Journal of Nuclear Materials*, vol. 420, pp. 347-361, 2012, doi: 10.1016/j.jnucmat.2011.09.032.
- [50] M. Morgenstein and T. J. Riley, "Hydration-rind dating of basaltic glass: a new method for archaeological chronologies," *Asian Perspectives*, vol. 17, pp. 145-159, 1974. [Online]. Available: <https://www.jstor.org/stable/42927872>.
- [51] J. L. Crovisier, T. Advocat, and J. L. Dussossoy, "Nature and role of natural alteration gels formed on the surface of ancient volcanic glasses (Natural analogs of waste containment glasses)," *Journal of Nuclear Materials*, vol. 321, pp. 91-109, 2003, doi: 10.1016/S0022-3115(03)00206-X.
- [52] R. C. Ewing and M. J. Jercinovic, "Natural analogues: their application to the prediction of the long-term behavior of nuclear waste forms," *Materials Research Society Symposium Proceedings*, vol. 84, pp. 67-83, 1987, doi: 10.1557/PROC-84-67.
- [53] N. C. Hyatt, C. L. Corkhill, M. C. Stennett, R. J. Hand, L. J. Gardner, and C. L. Thorpe, "The HADES Facility for High Activity Decommissioning Engineering & Science: part of the UK National Nuclear User Facility," *IOP Conference Series: Materials Science and Engineering*, vol. 818, p. 012022, 2020.